RSC Advances

PAPER

View Article Online
View Journal | View Issue

Cite this: *RSC Adv.*, 2022, **12**, 36103

Synthesis and characterization of rod-like amino acids/nanohydroxyapatite composites to inhibit osteosarcoma†

Zhengxiong Chen,[ac] Xinyu Wang,[*abc] Jing Luo,[ac] Bowen Zhang,[ac] Fei Shen,[ac] Binbin Li[*ac] and Jing Yang[d]

In this study, rod-like hydroxyapatite (HA) with uniform morphology and controllable particle size modified by doping with two different amino acids (alanine and threonine) was synthesized by a microwave hydrothermal method. The physical and chemical properties of the composites were tested by utilizing X-ray diffraction (XRD), Fourier transform infrared spectroscopy (FTIR), general thermogravimetric analysis (TG) and scanning electron microscopy (SEM). The SEM and XRD results show that the presence of amino acids (especially threonine) can significantly reduce the aspect ratio and crystallinity of hydroxyapatite. Pure hydroxyapatite and modified hydroxyapatite doped with two different proportions of amino acids were cultured with mouse osteoblasts (MC3T3-E1) for 1, 3 and 5 days, respectively, nanohydroxyapatite modified by threonine has better biocompatibility compared with pure hydroxyapatite. The amino acid-modified hydroxyapatite samples were co-cultured with osteosarcoma cells (MG63) for 1, 4 and 7 days, respectively, and showed better inhibitory effects on osteosarcoma cells. The nanohydroxyapatite doped with amino acids could be used as a potential drug that promotes bone repair and inhibits the growth of osteosarcoma cells.

Received 20th June 2022
Accepted 26th October 2022

DOI: 10.1039/d2ra03784j

rsc.li/rsc-advances

1. Introduction

Hydroxyapatite ($Ca_{10}(PO_4)_6(OH)_2$, HA) is a commonly used bone repair material, which is widely used in bone repair as well as tooth restoration and other surgical procedures.[1] Hydroxyapatite also has a promising application in drug delivery and cancer treatment, and hydroxyapatite has good biocompatibility, and its morphology, particle size and crystallinity are affected by many factors, including synthesis method, reaction conditions, reaction temperature and so on.[2–4] In addition, silver doped hydroxyapatite nanoparticles have good antibacterial effect, effectively preventing infection and eliminating bacteria in orthopedic surgery. Moreover, the hydroxyapatite synthesized by microwave hydrothermal method has better crystallinity and purity at low temperature.[5] Compared with the traditional chemical precipitation method, hydrothermal method and sol–gel method, the microwave hydrothermal method has apparent advantages in preparing nanohydroxyapatite, the microwave hydrothermal method has the advantages of fast heating speed, uniform heating of samples, uniform morphology of hydroxyapatite samples, smaller particle size, higher crystallinity, and less reaction time.[6–8] As the basic unit of human protein, amino acids play an essential role in the repair of bone tissue and the growth of osteoblasts. Nanohydroxyapatite has certain cytotoxicity. Therefore, amino acid modification of nanohydroxyapatite can be a potential research direction to reduce the toxicity of nanohydroxyapatite.[9]

In previous studies, nanohydroxyapatite particles with high dispersion can be prepared rapidly and in large quantities by microwave hydrothermal method combined with ultrasonic spray method. Ultrasonic spray method can make the liquid with higher initial kinetic energy uniformly dispersed in another reaction solution, reduce the aggregation of hydroxyapatite, and improve the dispersion of nanoparticles.[10–12] Some organic compounds, such as amino acids, gelatin and oxalic acid, can be directly absorbed by bone tissue to promote the growth of bone tissue. As the basic unit of protein, amino acids are easily absorbed by the human body and have a certain promotion effect on bone growth.[13–15] Alanine ($C_3H_7NO_2$, Ala) is the basic unit of protein and one of the 20 amino acids that make up human proteins. There are two different isomers, α-alanine and β-alanine. Because alanine has a methyl side chain, it can inhibit the growth of *C*-axis during the growth of

[a]*State Key Laboratory of Advanced Technology for Materials Synthesis and Processing, Wuhan University of Technology, Wuhan 430070, P. R. China. E-mail: wangxinyu@whut.edu.cn*

[b]*Foshan Xianhu Laboratory of the Advanced Energy Science and Technology Guangdong Laboratory, Xianhu Hydrogen Valley, Foshan 528200, P. R. China*

[c]*Biomedical Materials and Engineering Research Center of Hubei Province, Wuhan University of Technology, Wuhan 430070, P. R. China*

[d]*School of Foreign Languages, Wuhan University of Technology, Wuhan 430070, P. R. China*

† Electronic supplementary information (ESI) available. See DOI: https://doi.org/10.1039/d2ra03784j

hydroxyapatite, thus reducing the particle size of nanohydroxyapatite.[9,16] Since alanine is a necessary component of human protein, the introduction of alanine in the synthesis of hydroxyapatite will not increase the cytotoxicity of nanoparticles.[17–20] Threonine ($C_4H_9NO_3$, Thr) is an essential amino acid, mainly used in medicine, chemical reagents, food fortifier, and feed additives. Threonine can promote the metabolism of cells, promote the growth and development of cells, and regulate the conduction of human nerve cells, which plays an important role in the normal life activities of organisms.[2,11,13,16] The side chain of threonine is longer than that of alanine and contains hydroxyl groups. Therefore, threonine can participate in the synthesis process of hydroxyapatite and play a vital role in promoting cell growth and effectively promote the proliferation of osteoblasts.[21–24] There are a lot of negative charges on the surface of osteosarcoma cells, and the electrostatic repulsion between cells is significantly increased, so the osteosarcoma cells are easy to escape from the tumor tissue. Alanine and threonine have positive charged amino groups, which can reduce the electronegativity of osteosarcoma cells and avoid osteosarcoma cells escaping from tumor tissue, and they can also guide various targeted drugs to attack osteosarcoma cells.[7,20,25,26]

In our work, we hope that amino acids can effectively control the particle size of hydroxyapatite at the nanometer level, reduce abnormal grain growth, and improve the uniformity and dispersion of nanometer powders. And then we reveal that the combination of microwave hydrothermal method and ultrasonic spray method can prepare high-performance nanohydroxyapatite powder with more uniform morphology, higher crystallinity and higher biological activity. Furthermore, the differences in morphology and structure of hydroxyapatite modified by these two amino acids, alanine (Ala) and threonine (Thr) and their effects on cell growth are important contents of our research. In addition, we tested the physical and chemical features and biocompatibility of the materials and summarized the law of variation of the properties of amino acid-modified hydroxyapatite materials.

2. Experimental section

2.1. Synthesis of preparation materials

The process of preparing nanohydroxyapatite by microwave hydrothermal method and ultrasonic spray method is as follows: 90 ml 0.4 M $Na_2H(PO_4)\cdot 12H_2O$ and 100 ml 0.6 M $CaCl_2\cdot 2H_2O$ were completely dissolved in deionized water, continuously stirring for 30 min and keeping the temperature at 25 °C. Amino acids with different concentration gradients (0.3 M, 0.6 M, 0.9 M) were dissolved with calcium chloride solution, and then the disodium hydrogen phosphate solution was added into calcium solution, and the spray rate was maintained at 10 ml min^{-1} by a ultrasonic atomization instrument (UTA-6000, ATPIO, Nanjing). In this process, $NH_3\cdot H_2O$ was manually added to the mixture to maintain the pH of precursor solution at 10. And then stirring for 10 min at room temperature, the precursor solution was evenly added into Teflon reactors, and the solution volume in each container was kept at 100 ml. Teflon reactors were symmetrically placed into a high throughput microwave digestion-extraction-synthesis workstation (Master-14, SINEO, China) and they were heated by microwaves at 160 °C for 40 min. The heating process is divided into two steps. Firstly, the temperature was quickly raised to 120 °C at a rate of 10 °C min^{-1}. Secondly, when the temperature exceeds 120 °C, the heating rate was slightly decreased to 8 °C min^{-1}. Finally, the temperature was maintained at 160 °C for 40 min. The reaction samples were continuously washed and centrifuged at 12 000 rpm by distilled water until the pH of the supernatant was 7 and freeze-dried for 24 h to obtain nanohydroxyapatite samples. The different samples doped with different contents of alanine and threonine were respectively marked as HA-(n)A and HA-(n)T, where n (n = 0.5, 1, 1.5) is the value of the molar ratio (amino acid/Ca^{2+}). Pure hydroxyapatite was prepared by the same method when the calcium solution did not contain any amino acid, which was marked as HA.

2.2. Characterization

We utilized a BET system (ASAP 2460, Micromeritics, USA) to design a nitrogen adsorption experiment at 77 K, and the obtained hydroxyapatite samples were degassed for 10 h at 120 °C. The nitrogen adsorption and desorption isotherms were obtained to summarize the regulation of the surface area of the different samples. The surface area included the pore size and porous volume distribution, which were estimated by the Barrett–Joyner–Halenda (BJH) method. The crystallinity and diffraction characteristic peaks of the nanohydroxyapatite samples were measured by X-ray Diffraction (D8 Advance, Bruker, Germany). The wavelength of copper (Cu) X-ray target was marked as λ (λ = 0.154184 nm), and the samples was measured in the 2θ range of 10–80°. The crystallinity and microcrystalline size of the sample can be calculated based on the results tested by the XRD pattern. The formula for calculating the crystallinity of HA nanoparticles is as follows:[9]

$$X_C = 1 - (V_{112/300}/I_{300}) \quad (1)$$

where I_{300} is the intensity of the (300) reflection and $V_{112/300}$ is the intensity of the valley between the (112) and (300) diffraction peaks for HAP. Meanwhile, the mean crystallite size of the sample was evaluated by using the Scherrer equation:[9]

$$D_{hkl} = k\lambda/\beta_{1/2}\cos\theta \quad (2)$$

where k is a constant chosen as 0.9, λ is the wavelength of the Kα radiation of copper (λ = 0.15418 nm), and $\beta_{1/2}$ is the line width which is at the full width at half maximum (FWHM) of a characteristic peak. Fourier-Transform Infrared Spectroscopy (FTIR, Nexus, Thermo Nicolet, USA) was provided to test the spectrum by the KBr pellet method, of which the wavenumber range is from 400 cm^{-1} to 4000 cm^{-1}, and the information of the functional groups in the different samples is given by the FTIR method. A thermogravimetric analyzer (STA449F3, NETZSCH, Germany) was used to explore the mass change at different temperatures of obtained samples. The heating process was set

to a heating rate of 10 °C min^{-1}, which was from room temperature to 1000 °C and the samples were placed in a nitrogen atmosphere. Scanning electron microscope (SEM, S-4800, HITACHI, Japan) was utilized to observe the surface and morphology structure of the obtained hydroxyapatite samples. Different samples were evenly dispersed in ethanol and the concentration of products were 1 mg ml^{-1}. The liquid samples were dropped onto the aluminum foil and spray the sample with gold after the alcohol evaporates deposited and then the hydroxyapatite samples were observed by SEM.

The Cell Counting Kit-8 (CCK-8; Beyotime, China) was utilized to evaluate the cytotoxicity of hydroxyapatite products and the instructions of CCK-8 were given to test for the cytotoxicity of samples. The mouse osteoblast cell line (MC3T3-E1) was used as the suitable cell for investigating the cytotoxicity of hydroxyapatite products. The samples were sterilized by damp-heat sterilization to obtain the different extract solution. The sterilization conditions were set to 115 °C, 1.2 MPa for 35 min. The sterilized samples were dispersed in α-MEM medium (Hyclone, China) respectively, and the concentration was kept at 2 mg ml^{-1}. The liquid samples were shaken in a shaking table (SHA-BA, Jiangsu) for 12 h at a temperature of 37 °C. The samples were centrifugated at 10 000 rpm for 12 min by a centrifuge (TG16-WS, cence, China), and the supernatant was finally collected for reserve, respectively. 10% of fetal bovine serum (FBS, Biological Industries) and 1% of penicillin and streptomycin (Hyclone, China) were added to 89% of the prepared supernatant to obtain the extract solution which was stored at −15 °C. The MC3T3-E1 cells were inoculated in a 96-well plate and the density was 4000 cells per well. The cells were cultured at 37 °C with 5% CO_2 for 24 h. The 100 μl α-MEM medium including 10% of fetal bovine serum and 1% of penicillin and streptomycin was replaced by the extract solution in each well. The MC3T3-E1 cells were cultured for 1 day, 3 days and 5 days, respectively, the extract solution was substituted by the mixture of 10 μl CCK-8 and 100 μl the α-MEM medium in each well and incubated for 2 h. Then, the optical density of each well was measured by an enzyme standard instrument (Varioskan LUX, Thermo Fisher Scientific, America) at a wavelength of 450 nm. Each sample was repeated four times. In the clean table, open the six-hole plate and place the sterilization cover glass. The cell suspension drops (100 000 cells per well) were added to the cover glass and placed in an incubator with CO_2 concentration of 5% at 37 °C until the cells became fixed (about 2 h). Add 2 ml of cell culture medium and continue to culture for about 6 h. Remove the medium and wash with PBS for 3 times, wash for 5 min each time. And then 4% paraformaldehyde was fixed for 30 min, and wash with PBS 3 times, 5 min each time. After the slide was dried, draw a circle with a pap pen (Liquid Blocker, China) on the center of the cover glass where the cells were evenly distributed to prevent the liquid from flowing away. Then add 100 μl of phalloidin, incubate it at room temperature for 2 h and wash it with PBS 3 times, 5 min each time. The slides were washed with PBS (pH = 7.4) 3 times, 5 min each time. After the removal of PBS, DAPI solution was added to the ring and incubated at room temperature in the dark for 10 min. The slides were washed with PBS (pH = 7.4) 3 times, 5 min each. After the slide is slightly shaken dry, the cell side down is sealed on the slide with an anti-fluorescence quenching sealing tablet to seal the slide. Photographs were taken using a confocal laser microscope (Olympus, FV3000, Japan).

All sterilized samples were dispersed in MEM medium (Hyclone, China) with 10% of fetal bovine serum and 1% of penicillin and streptomycin, respectively, and the concentration was kept at 2 mg ml^{-1}. In the same way, the HA-0.5T and HA-1.5T samples were configured as culture medium with different concentrations, and the concentrations were set as 1 mg ml^{-1}, 2 mg ml^{-1}, and 3 mg ml^{-1}, respectively. All samples were mixed evenly with the MEM medium and stored at 4 °C. The mouse osteosarcoma cells (MG63) were inoculated in a 96-well plate and the density was 3000 cells per well. The cells were cultured at 37 °C with 5% CO_2 for 24 h. The 100 μl MEM medium including 10% of fetal bovine serum and 1% of penicillin and streptomycin was replaced by the culture solution in each well, and replace the culture solution with new culture solution every three days. The MG63 cells were cultured for 1 day, 4 days and 7 days, respectively. The culture solution was substituted by the mixture of 10 μl CCK-8 and 100 μl the α-MEM medium in each well and incubated for 2 h. Then, the optical density of each well was measured by an enzyme standard instrument (Varioskan LUX, Thermo Fisher Scientific, America) at a wavelength of 450 nm. Each sample was repeated three times. The Calcein-AM/PI Double Stain Kit (Yeasen, Shanghai, China) was utilized to stain the MG63 cells on the seventh day, and 50 μl dyeing solution was added into each well. The fluorescent inverted microscope was utilized to take photographs and the magnification was 100 times.

3. Results and discussion

The results of nitrogen adsorption and desorption isotherms are shown in Fig. 1. Adsorption hysteresis loops appeared in the different samples, which can indicate that all the obtained HA samples are mesoporous materials. The BJH method was utilized to measure the porous size and porous volume of different samples and in Table 1, the specific surface area (S_{BET}) of the synthesized samples were shown. The specific surface area of nanocrystals containing amino acids was significantly higher than that of pure hydroxyapatite. With the increase of threonine content, the specific surface area of the sample gradually decreased, which is from 109 m^2 g^{-1} to 99 m^2 g^{-1}. This indicates that the specific surface area of nano-hydroxyapatite will change after the addition of amino acids. The porous size of samples gradually decreased with the content of amino acids. The specific surface area of the samples supplemented with threonine was higher than the samples supplemented with alanine. The pore size of the material is affected by the amino acid molecule.[1,9,19] The nanometer hydroxyapatite with different pore sizes and specific surface areas can be prepared by controlling the amount of amino acid added.

In Fig. 2, the X-ray diffraction patterns of obtained nano-hydroxyapatite materials are shown. Compared with the JCPDS

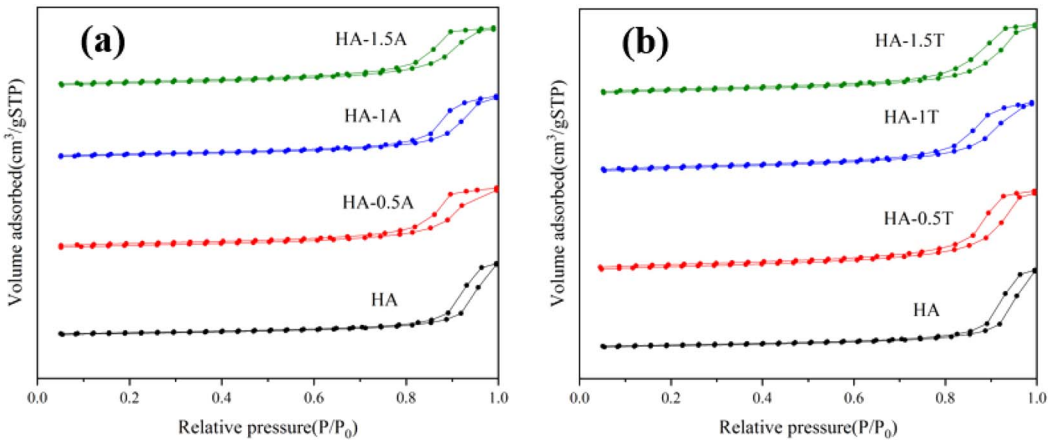

Fig. 1 Nitrogen adsorption and desorption isotherms for the different HA samples.

Table 1 The results of specific surface area of all obtained samples

Sample	S_{BET} (m^2 g^{-1})	Pore volume (cm^3 g^{-1})	Pore size (nm)
HA	73	0.466815	22.2
HA-0.5A	97	0.391749	13.8
HA-1A	89	0.401319	15.4
HA-1.5A	94	0.379435	12.6
HA-0.5T	109	0.475456	14.4
HA-1T	105	0.419612	13.1
HA-1.5T	99	0.416013	14.2

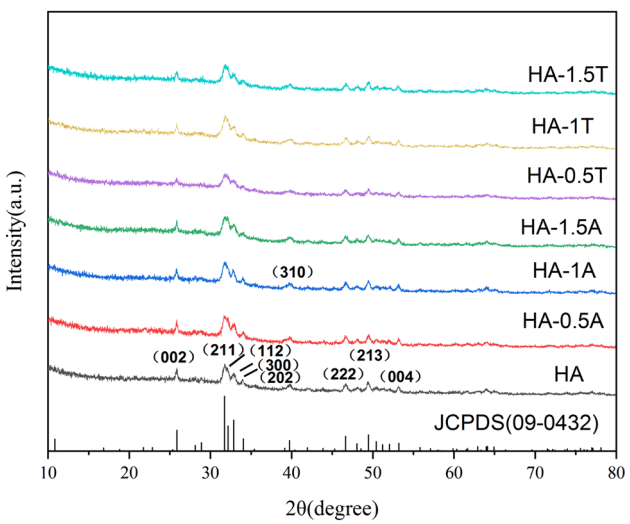

Fig. 2 XRD patterns of all obtained samples doped with Ala and Thr.

(09-0432), the presence of characteristic peaks for hydroxyapatite and the absence of other miscellaneous peaks indicates that the prepared material is pure hydroxyapatite. The diffraction characteristic peaks including the (002), (211), (112), (300), (202), (310), (222), (213), and (004) crystal faces can validly prove that the samples belong to the hexagonal hydroxyapatite.[2,6,9]

After the samples were doped with two amino acids, alanine and threonine, the intensity of characteristic peaks was slightly reduced, and the full width at half maximum broadened, which reveals that the growth of nanocrystals was inhibited. The final results are recorded in Table 2. The crystallinity of the pure hydroxyapatite is 0.92, and the crystallinity of the samples containing alanine or threonine was lower than that of the pure hydroxyapatite samples, which depends on the amount of amino acid doped. For the samples which were doped by alanine, the crystallinities of HA-0.5A, HA-1A, and HA-1.5A were 0.87, 0.84, and 0.71, respectively. For the product of the presence of threonine, the crystallinities of HA-0.5T, HA-1T, and HA-1.5T were 0.85, 0.73, and 0.81, respectively. With the increase of threonine concentration, the variation trend of the crystallinity of the sample is firstly increased, then decreased and finally increased.

The different influence of Ala and Thr in the mean grain size is revealed in Fig. 3. When the content of alanine and threonine doped in the samples increased, the grain size of the HA materials decreased obviously, especially in (002) and (213). For the sample HA-1.5T, the value of grain size was decreased about 60% and 65%, comparing with the pure HA in (002) and (213). Similarly, for the HA-1.5A sample, the grain size in (002) and (214) also reveals the same trend. Doping of two amino acids, the crystallinity of hydroxyapatite powders have a certain degree of decline. This is because the hydroxyapatite with obvious

Table 2 The results of grain size and crystallinity of the prepared samples

Sample	$\beta_{1/2}$ (002)	D(002)	$\beta_{1/2}$ (213)	D(213)	Crystallinity (X_c)
HA	0.202	46.6	0.301	30.9	0.92
HA-0.5A	0.249	35.7	0.344	26.5	0.87
HA-1A	0.276	31.7	0.370	24.5	0.84
HA-1.5A	0.278	31.4	0.423	21.3	0.71
HA-0.5T	0.230	39.3	0.392	23.1	0.85
HA-1T	0.250	35.6	0.416	21.7	0.73
HA-1.5T	0.301	28.7	0.447	20.1	0.81

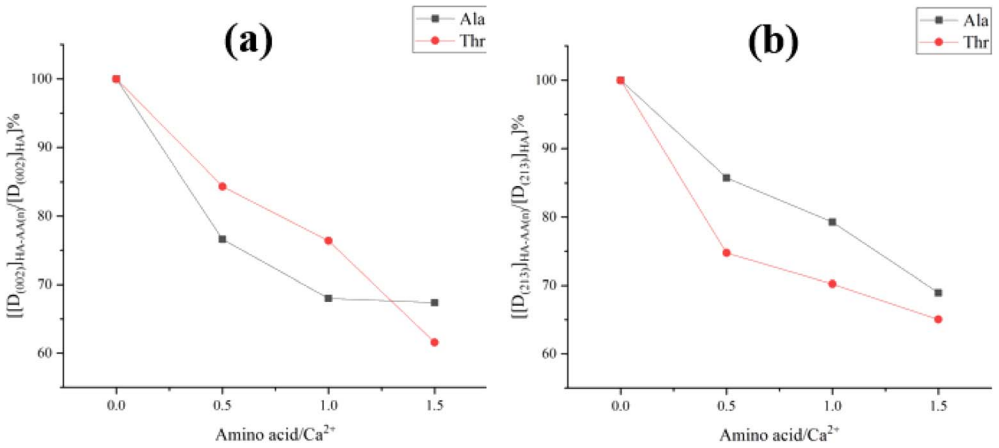

Fig. 3 The distinct of the different contents of Ala and Thr in the grain size D(002) (a) and D(213) (b).

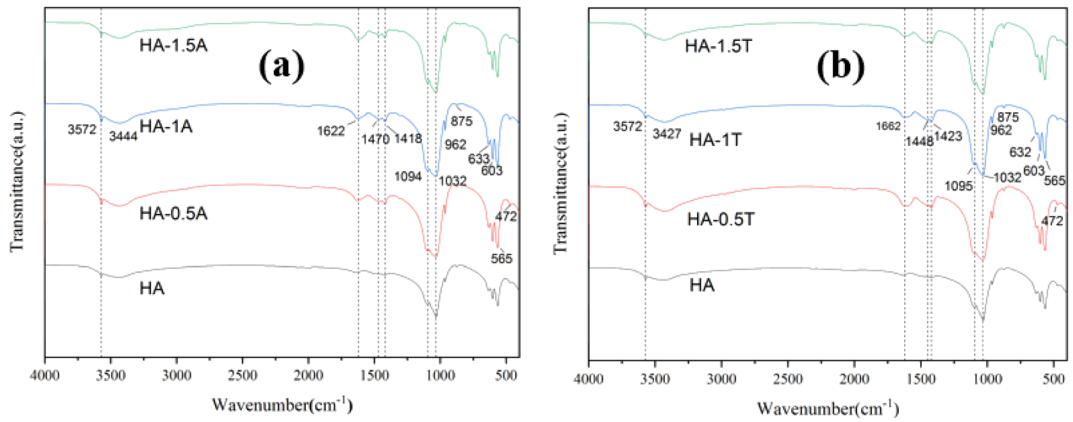

Fig. 4 The FTIR spectra of the obtained HA samples doped with Ala (a) and Thr (b).

electrostatic adsorption between amino acids, such as electrostatic adsorption between Ca^{2+} and COO^{-} will involve amino acids in the growth of hydroxyapatite process, which affect the degree of crystallinity of the sample. This electrostatic effect inhibits the binding between calcium ions and phosphate ions. When more calcium ions are combined with carboxyl group, the atomic number ratio of calcium to phosphorus in the sample is less than 1.67, resulting in the crystallinity and grain size declined. Therefore, amino acids can inhibit crystal growth in the preparation of hydroxyapatite.[26,27] The crystallinity of hydroxyapatite samples synthesized by microwave heating is higher than 70% due to the accelerated thermal movement of

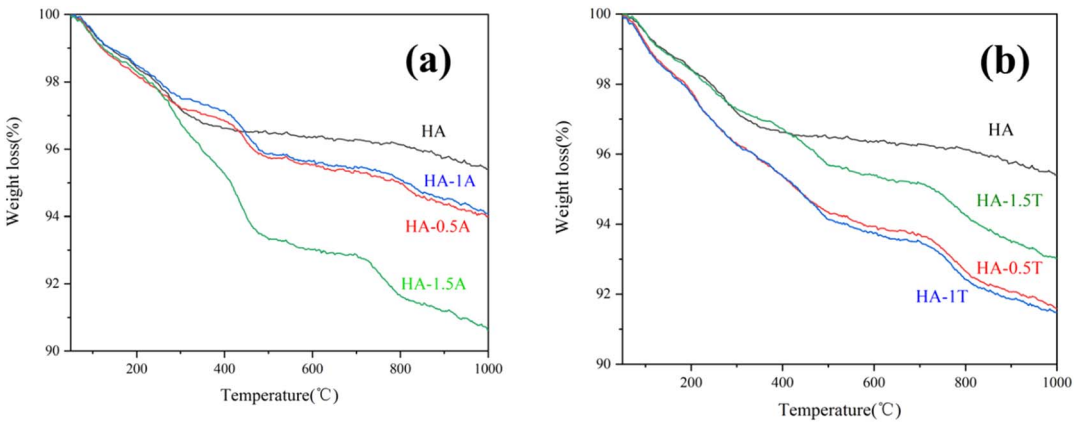

Fig. 5 TG of the obtained HA samples doped with Ala (a) and Thr (b).

Table 3 TG results and analysis of samples at different temperature ranges

Sample	First loss (wt%) (50–200 °C)	Second loss (wt%) (200–1000 °C)
HA	1.59	2.99
HA-0.5A	1.81	4.19
HA-1A	1.49	4.39
HA-1.5A	1.67	7.66
HA-0.5T	2.15	6.22
HA-1T	2.17	6.26
HA-1.5T	1.61	5.36

molecules and ions and more uniform and fast hydrothermal reaction. Therefore, the crystallinity of the nanohydroxyapatite is higher and the heating time is shorter than that of the traditional hydrothermal method.

The FTIR spectra of the samples HA, HA-0.5A, HA-1A, and HA-1.5A are indicated by Fig. 4a, respectively. The two amino acids are doped into the nanohydroxyapatite, which is strongly demonstrated. In the hydroxyapatite spectrum, the infrared absorption peak confirms the presence of hydroxyl groups, the absorption peaks at 3572 cm^{-1} and 633 cm^{-1} are stretching vibration peak and contraction vibration peak of the hydroxyl groups, which can strongly prove that OH^- is in present of the samples. The peaks at 1094 cm^{-1}, 1032 cm^{-1} ($\nu 3$, asymmetric

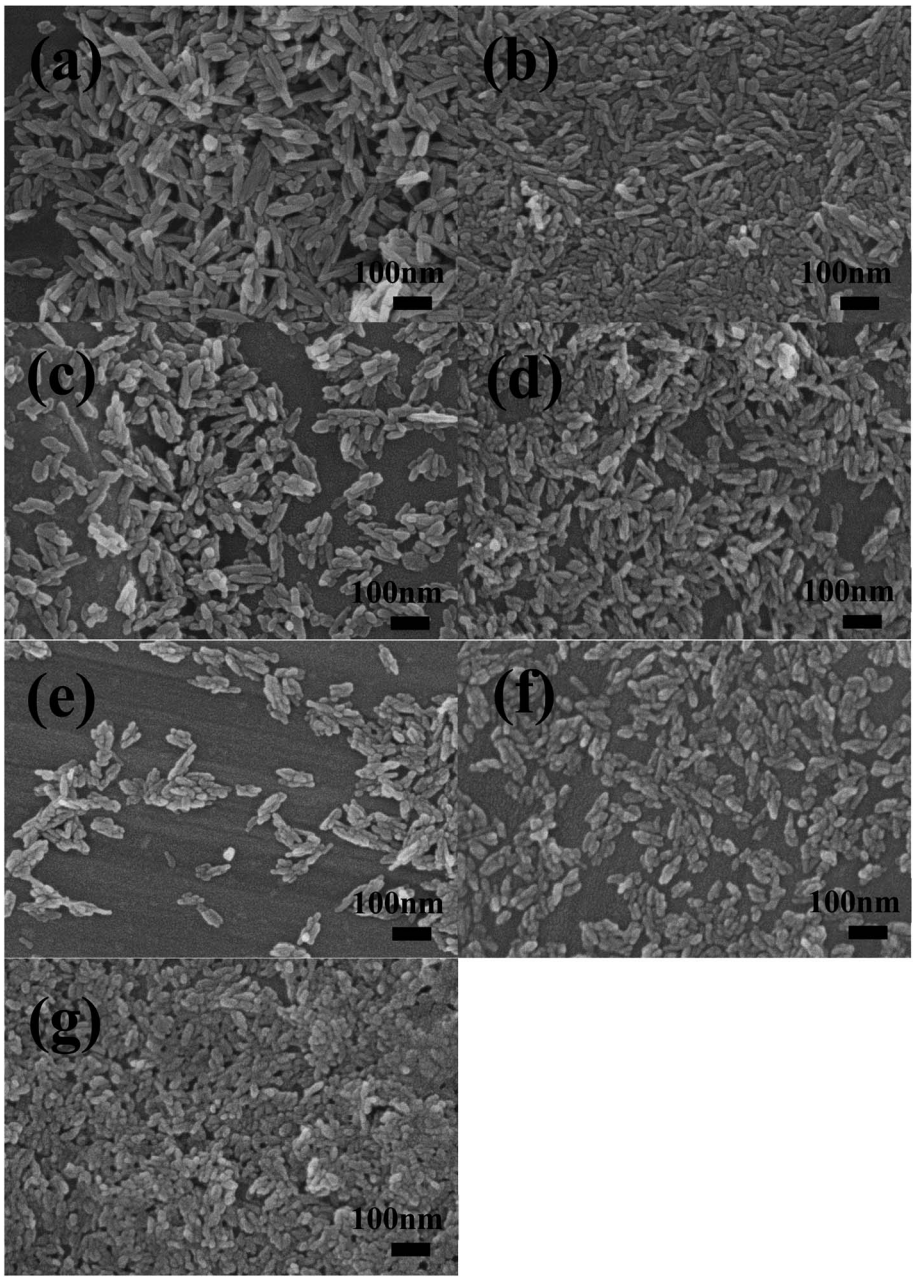

Fig. 6 SEM image of the different samples: HA (a), HA-0.5A (b), HA-1A (c), HA-1.5A (d), HA-0.5T (e), HA-1T (f), HA-1.5T (g).

stretching), 962 cm^{-1} (ν1, symmetric stretching), 603 cm^{-1}, and 565 cm^{-1} (ν4, bending) can testify to the presence of phosphate ions. In addition, carbonate ions also exist in the samples, this is because the vibrational peaks appeared in 875 cm^{-1} (ν2, out-of-plane bending) and 1418 cm^{-1} (ν3). It may be caused by carbon dioxide entering the solution, producing carbonate ions

Table 4 The results of average length and width of the obtained samples

Sample	HA	HA-0.5A	HA-1A	HA-1.5A	HA-0.5T	HA-1T	HA-1.5T
Length	86	44	48	49	45	49	40
Width	23	15	20	20	19	22	20

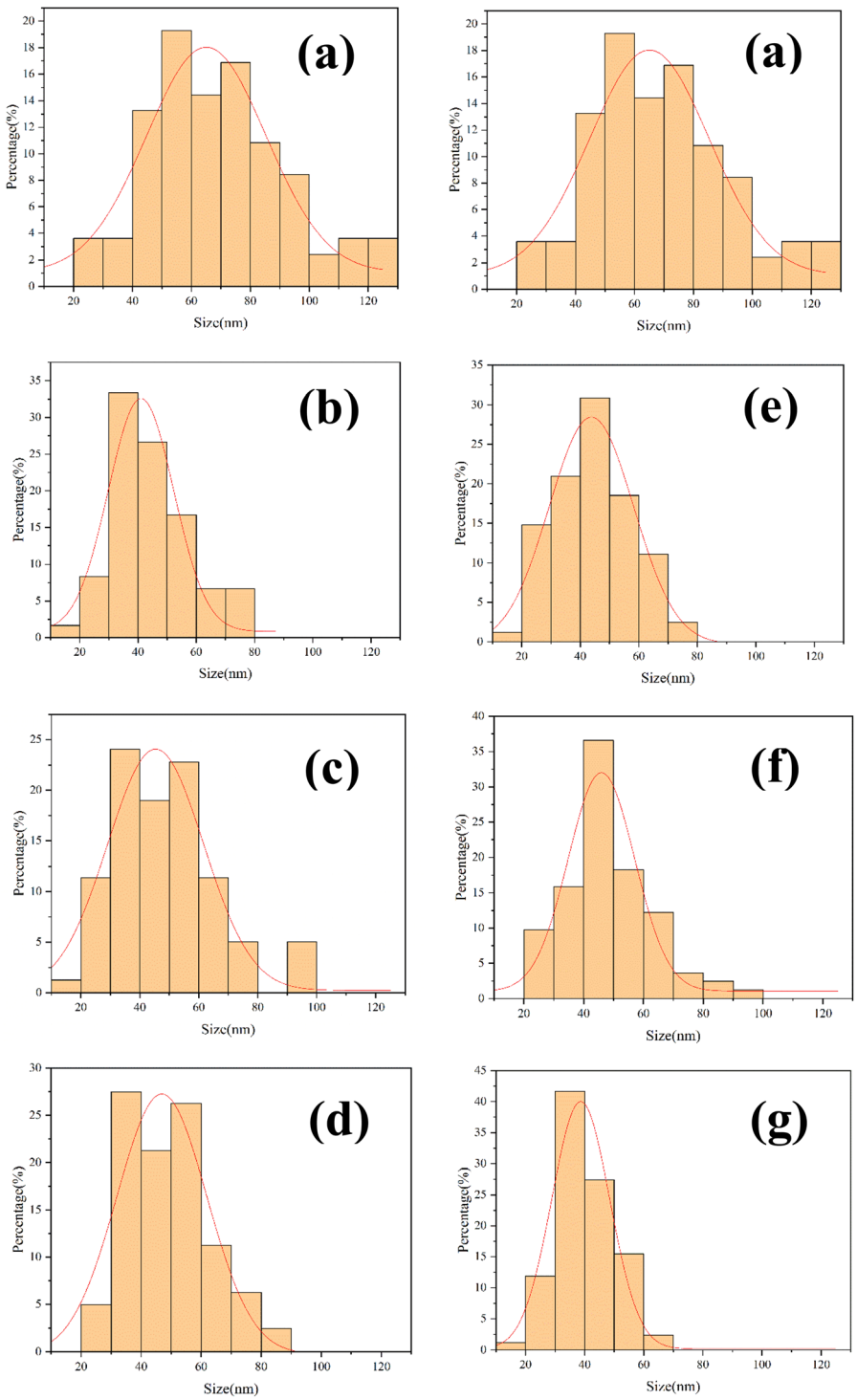

Fig. 7 Different results of grain size distribution of the obtained samples: HA (a), HA-0.5A (b), HA-1A (c), HA-1.5A (d), HA-0.5T (e), HA-1T (f), HA-1.5T (g).

and combining with calcium ions into the nanohydroxyapatite sample.

The amino acids are involved in the crystal growth process, the absorption peaks at 1400–1430 cm^{-1} and 1450–1485 cm^{-1} correspond to $-COO^-$ and $-NH_4^+$, respectively, which prove the existence of chemically bonded amino acids.[28,29] As shown in Fig. 4b, the peaks at 1418 cm^{-1}, 1423 cm^{-1} are different from the HA-1A and HA-1.5A samples, revealing the Ala and Thr's distinctness affecting the HA powders. The FTIR study shows that a small number of amino acids were adsorbed by the nanohydroxyapatite, while other amino acids were bound to the nanohydroxyapatite to form part of the hydroxyapatite, and a small amount of carbonate was also present in the sample. The content of carbonate is generally not more than 5%, the higher the content of carbonate in hydroxyapatite, the worse the thermal stability of the sample, the crystallinity will also be reduced.

The thermogravimetric (TG) results of the HA, HA-0.5A, HA-1A, HA-1.5A, HA-0.5T, HA-1T, and HA-1.5T samples reveal the process and change trend of the mass loss at different temperatures in Fig. 5. When the temperature is between 50 °C and 200 °C, the water of crystallization in the hydroxyapatite sample is heated and vaporized. When the temperature is higher than 200 °C, the amino acid molecules adsorbed on the surface of the sample doped with two kinds of amino acids will decompose at high temperature, resulting in the decrease of the total mass of the sample, as is shown in the Fig. 5. In Table 3, the percentage variation of mass loss over different temperature ranges can be clearly shown. Obviously, when the temperature increases from 200 °C to 1000 °C, the mass loss of nanohydroxyapatite samples doped with amino acids is more. The experimental data show that there is a small number of amino acids in the hydroxyapatite sample, and the samples lose water of crystallization after heating, and the total mass of the samples are reduced due to the decomposition of amino acids after heating. When the temperature increases from 200 °C to 1000 °C, the percentage of sample (HA-1.5A and HA-1.5T) mass loss is 7.66% and 5.36%, respectively. This was mainly due to the decomposition of amino acids present in the samples at high temperature, which bonded with the hydroxyapatite inside the hydroxyapatite rather than adsorbed on the surface of the sample.

In Fig. 6, all the HA samples are rod-like nanohydroxyapatite powder, and the dispersibility of the samples was improved by doping amino acids. Compared with pure hydroxyapatite, hydroxyapatite doped with amino acids has smaller particle size, better dispersion and smaller grain size. The crystal boundary of pure hydroxyapatite is very clear and the agglomeration is serious, while the crystal boundary of hydroxyapatite modified by doping amino acids is fuzzier, which indicates that the crystallinity of samples doped with amino acids decreases, the dispersibility is improved to a certain extent, and the

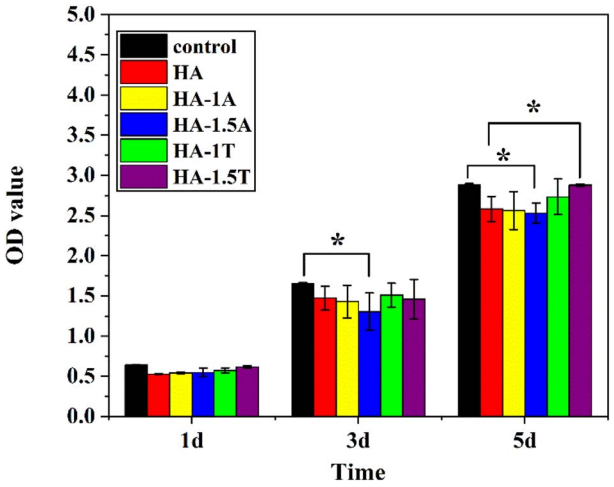

Fig. 8 The CCK8 results of MC3T3-E1 cells cultured with different leaching solution of obtained samples for 1, 3 and 5 days. (*) — represents statistically significant ($p < 0.05$).

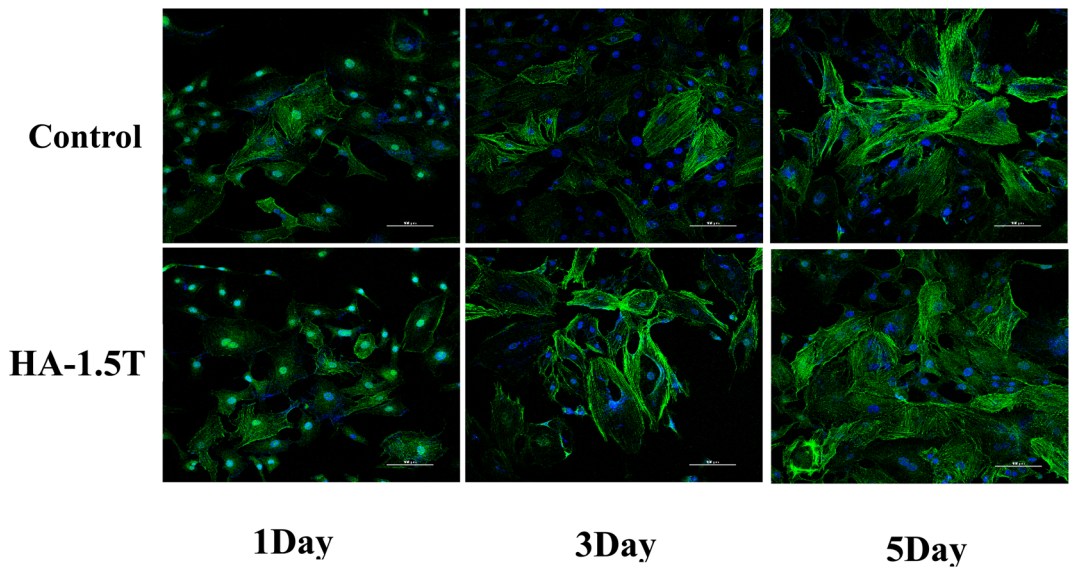

Fig. 9 The morphology and structure of MC3T3-E1 cells cultured with leaching solution of HA-1.5T for 1, 3 and 5 days.

specific surface area of samples is relatively large, which is consistent with the previous experimental results.

As is indicated in Fig. 7 and Table 4, one hundred nanoparticles are chosen to measure the length and width from different SEM images of all HA samples. Then the grain size and particle size distribution of the synthesized samples are recorded by using the ImageJ software.

With the increase of amino acid content, the morphology of hydroxyapatite samples gradually becomes shorter and coarser, and the dispersion is improved. A small amount of nanoparticle aggregation appeared in the pure HA samples. In the process of sample synthesis and preparation, amino acids produce acetate ions and calcium ions in hydroxyapatite coordination binding, blocking the combination of calcium ions and phosphate ions so that the crystal growth process of the sample is inhibited. The significant decrease in the length of nanoparticles indicates that the growth of samples along the *C*-axis is inhibited, which is related to the content of amino acids added.[28,30,31] Under the electrostatic interaction of Ca^{2+} and COO^{-}, the amount of Ca^{2+} binding with PO_4^{3-} decreases, and the ratio of calcium to phosphorus in the formed hydroxyapatite is less than 1.67, and the growth of hydroxyapatite is inhibited. The length of particle (HA-1.5T) is the smallest in all products, which is about 40 nm.

The optical density value is related to cell proliferation. The higher the optical density value, the more cell proliferation. As is indicated in Fig. 8, there was no significant difference in the optical density value of all samples on the first day. The results show that the cell growth of all samples was close to the normal cell growth. The different samples began to show differences in optical density values on the third day. The optical density value of the pure hydroxyapatite sample is slightly lower than that of the control group, indicating that the pure hydroxyapatite sample has a certain inhibitory effect on cell proliferation, which could be caused by the nanoparticles being phagocytized by MC3T3-E1 cells. Compared with the control group, the optical density values of HA-1.5A is significantly lower, indicating hydroxyapatite doped with alanine inhibits cell proliferation. But the optical density of HA-1T and HA-1.5T are slightly higher than that of pure HA sample. The differences of optical density values between pure hydroxyapatite and the hydroxyapatite modified with alanine and threonine are not very obvious, and the reason may be that the number of cells was very small and the cell proliferation rate was very slow until the third day. The result was clearly indicated on the 5th day, the optical density of HA-1.5T was significantly higher than that of the pure HA group, and the optical density of HA-1.5T is similar to that of the control group, indicating threonine can reduce the cytotoxicity of hydroxyapatite to MC3T3-E1 cells. The optical density of HA-1.5A was significantly lower than that of the control group, indicating the hydroxyapatite doped with alanine

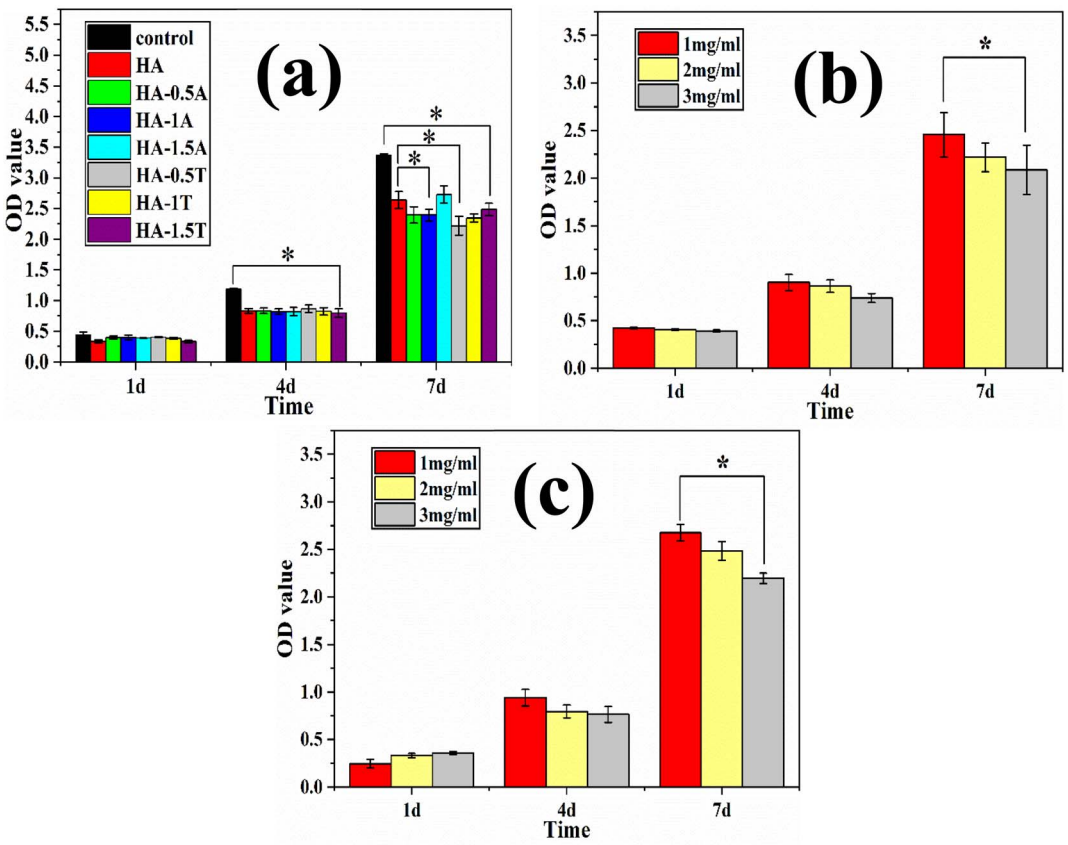

Fig. 10 The CCK8 results of MG63 cells cultured with different culture solution of obtained samples for 1, 4 and 7 days. (a) The effect of different samples on cells. (b) The effect of different concentration of HA-0.5T samples on cells. (c) The effect of different concentration of HA-1.5T samples on cells. (*) — represents statistically significant ($p < 0.05$).

was potentially toxic to cells and inhibited cell proliferation. Nanoydroxyapatite is easily engulfed by osteoblasts, causing certain cytotoxicity. After amino acid-modified hydroxyapatite is phagocytized by cells, amino acids are used as nutrients for cells and have the effect of promoting cell growth. Therefore, amino acid-modified nanohydroxyapatite has higher biocompatibility than pure hydroxyapatite. The experimental result reveals that the effect of threonine-modified hydroxyapatite is better than that of alanine.

As is shown in Fig. 9, the morphology and structure of MC3T3-E1 cells cultured with leaching solution of HA-1.5T for 1, 3 and 5 days are similar to control group. It is clearly shows that HA-1.5T has good biocompatibility and it can be a potential drug carrier for bone tissue repair, which is due to that it has smaller particle size and higher specific surface area than pure hydroxyapatite prepared by traditional method. On the 3rd day, the cells cultured with extracts of HA-1.5T are larger than the control group, but the number of cells are fewer. On the 5th day, the proliferation of cells cultured with extracts of HA-1.5T is similar than the control group, and the cells are larger than the control group. It is consistent with the results of CCK8 assay. Threonine can be used by cells as an essential nutrient, so the threonine modified hydroxyapatite can promote the growth of cell volume and promote the bone repair of the organism.

As is shown in Fig. 10a, all samples of hydroxyapatite had obvious inhibitory effects on MG63 cells on the 4th day, and the optical density value of all hydroxyapatite samples were similar. On the 7th day, compared with pure hydroxyapatite, HA-1A and HA-0.5T showed better inhibitory effects on MG63 cells. For the hydroxyapatite samples doped with threonine, the inhibitory effect of the samples on cells was more obvious with the decrease of amino acid doping amount. The HA-0.5T has the strongest inhibitory effect on MG63 cells. The reason is that particle size of nanohydroxyapatite modified by amino acid is smaller than pure hydroxyapatite and the amino acids are the nutrients of cells, it is easier to be phagocytosed by MG63 cells, so the ability of nanohydroxyapatite modified by amino acid to inhibit osteosarcoma cells is improved. The effects of different concentrations of HA-0.5T and HA-1.5T samples on MG63 cells were indicated in Fig. 10b and c. With the increase of sample concentration, the inhibitory effect of sample on cells was more obvious. The inhibitory effect of 2 mg ml^{-1} of HA-0.5T was slightly stronger than 2 mg ml^{-1} of HA-1.5T on the 7th day. By increasing the concentration of the samples, the toxicity of samples to cells could be improved and the growth of tumor cells could be inhibited.

The morphology and distribution of living and dead MG63 cells after 7 days of co-culture with the different samples were clearly shown in Fig. 11. Nanoydroxyapatite samples modified by amino acids had stronger inhibitory effects on osteosarcoma cells than pure hydroxyapatite samples. The results of MG63 cells staining were consistent with CCK8 results of MG63 cells. It was proved that hydroxyapatite modified by amino acids had good inhibitory effect on cells. The inhibitory effect of the HA-0.5T sample was the best.

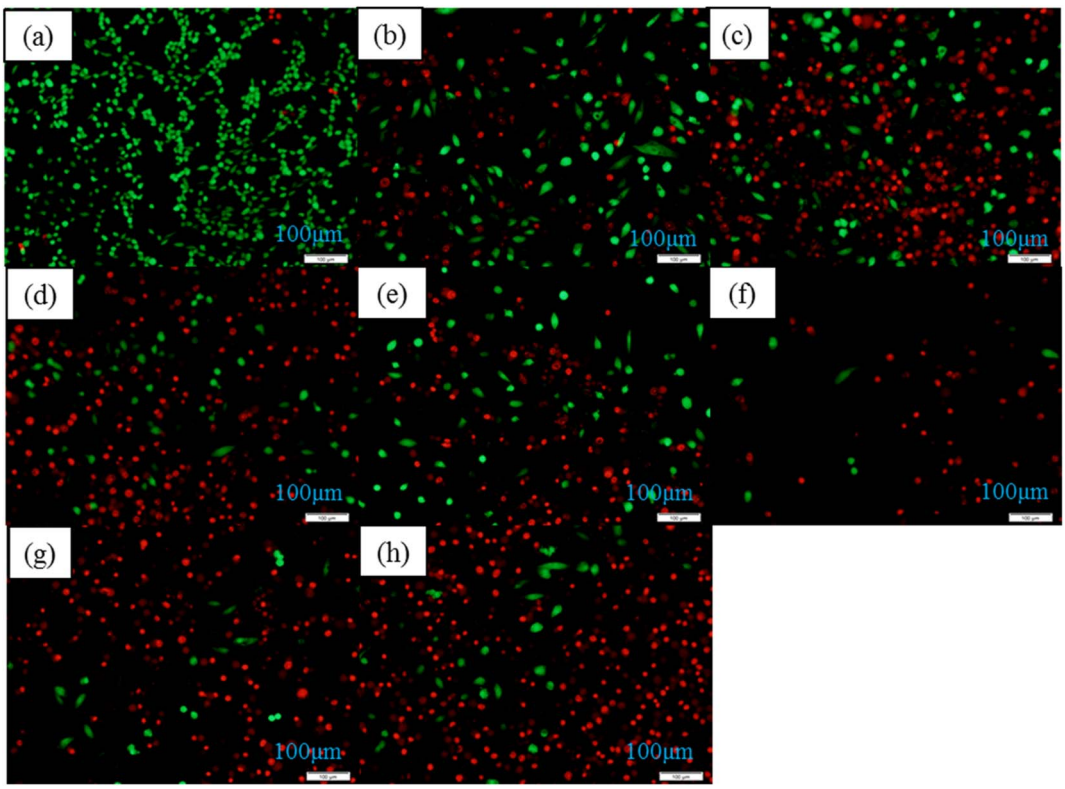

Fig. 11 The MG63 cells staining results of different samples for 7 days: control group (a), HA (b), HA-0.5A (c), HA-1A (d), HA-1.5A (e), HA-0.5T (f), HA-1T (g), HA-1.5T (h).

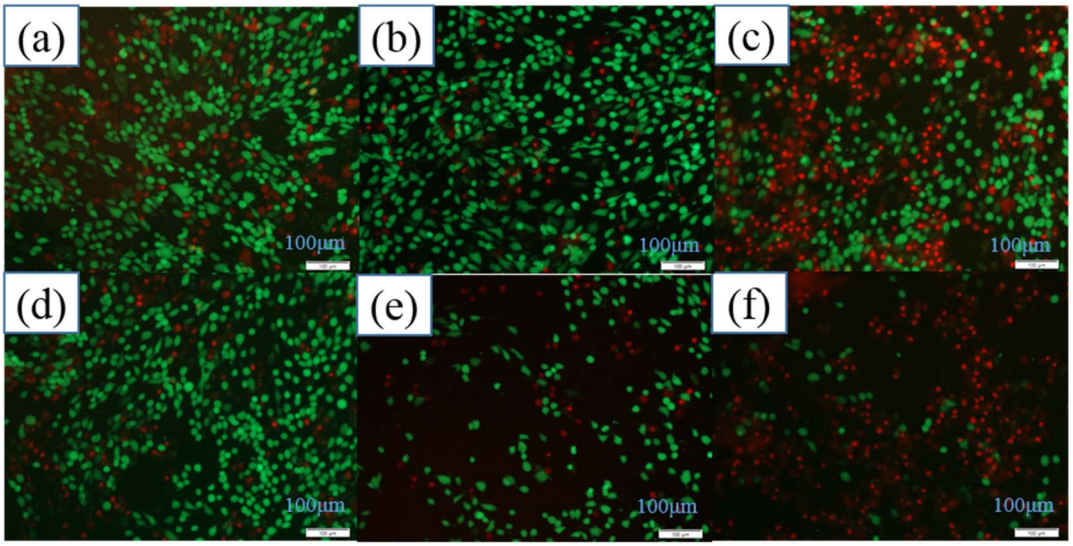

Fig. 12 The MG63 cells staining results of HA-0.5T and HA-1.5T samples of different concentrations for seven days: 1 mg ml^{-1} HA-0.5T (a), 2 mg ml^{-1} HA-0.5T (b), 3 mg ml^{-1} HA-0.5T (c), 1 mg ml^{-1} HA-1.5T (d), 2 mg ml^{-1} HA-1.5T (e), 3 mg ml^{-1} HA-1.5T (f).

The effects of different concentration of samples on MG63 cells were indicated in Fig. 12. With the concentration of the samples in the culture medium increasing, the inhibitory effect of MG63 cells was more obvious. The inhibition effect of the HA-0.5T sample was better than HA-1.5T sample.

4. Conclusions

In this paper, nanohydroxyapatite materials doped with two amino acids (alanine, threonine) were prepared by microwave hydrothermal method. The results of this research showed the following conclusions: (a) compared with pure hydroxyapatite, the grain size of nanohydroxyapatite doped with amino acids decreases obviously, and the specific surface area of the sample increases, which has better dispersion; (b) the crystallinity of nanohydroxyapatite doped with amino acids is lower than that of pure hydroxyapatite, but the specific surface area of nanohydroxyapatite is significantly higher than that of pure hydroxyapatite; (c) among all the samples, the threonine-doped hydroxyapatite materials show the high biocompatibility, especially HA-1.5T, which has almost no cytotoxicity to osteoblast cells; (d) the nanohydroxyapatite doped with amino acids has stronger inhibitory effect on osteosarcoma cells than the pure hydroxyapatite, and with the increase of sample concentration, the inhibitory effect on osteosarcoma cells became stronger.

Amino acid modified hydroxyapatite than pure hydroxyapatite has smaller size, higher specific surface area, can be used as a carrier of drugs used in bone repair treatment such as cosmetic surgery and bone healing process, because of threonine modified hydroxyapatite cytotoxicity significantly lower than the pure hydroxyapatite, so for bone repair materials used in the human body since the healing process of bone and it can effectively inhibit the growth of osteosarcoma cells as a potential antitumor drug during recovery from osteosarcoma surgery.

Conflicts of interest

There are no conflicts to declare.

Acknowledgements

This work was supported by the National Key R&D Program of China (No. 2017YFC1103800), the Foshan Xianhu Laboratory of the Advanced Energy Science and Technology Guangdong Laboratory (No. XHT2020-010) and the Major Special Projects of Technological Innovation of Hubei Province (No. 2017ACA168).

References

1 J. Tao, Y. Shin, R. Jayasinha, G. W. Buchko, S. D. Burton, A. C. Dohnalkova, Z. Wang, W. J. Shaw and B. J. Tarasevich, The Energetic Basis for Hydroxyapatite Mineralization by Amelogenin Variants Provides Insights into the Origin of Amelogenesis Imperfecta, *Proc. Natl. Acad. Sci. U. S. A.*, 2019, **116**(28), 13867–13872.

2 Z. Cai, X. Wang, Z. Zhang, Y. Han, J. Luo, M. Huang, B. Zhang and Y. Hou, Large-Scale and Fast Synthesis of Nano-Hydroxyapatite Powder by a Microwave-Hydrothermal Method, *RSC Adv.*, 2019, **9**(24), 13623–13630.

3 D. Kuang, F. Jiang, F. Wu, K. Kaur, S. Ghosh, S. C. Kundu and S. Lu, Highly Elastomeric Photocurable Silk Hydrogels, *Int. J. Biol. Macromol.*, 2019, **134**, 838–845.

4 Z. Wu, Z. Zhou and Y. Hong, Gelcasting of through-Pore Hydroxyapatite Ceramics, *J. Eur. Ceram. Soc.*, 2019, **39**(2–3), 547–553.

5 S. Lamkhao, M. Phaya, C. Jansakun, N. Chandet, K. Thongkorn, G. Rujijanagul, P. Bangrak and C. Randorn, Synthesis of Hydroxyapatite with Antibacterial Properties Using a Microwave-Assisted Combustion Method, *Sci. Rep.*, 2019, **9**(1), 4015.

6 S. Dey, M. Das and V. K. Balla, Effect of Hydroxyapatite Particle Size, Morphology and Crystallinity on Proliferation of Colon Cancer Hct116 Cells, *Mater. Sci. Eng. C Mater. Biol. Appl.*, 2014, **39**, 336–339.

7 C. João, R. Almeida, J. Silva and J. Borges, A Simple Sol-Gel Route to the Construction of Hydroxyapatite Inverted Colloidal Crystals for Bone Tissue Engineering, *Mater. Lett.*, 2016, **185**, 407–410.

8 T. Kang, X. Hua, P. Liang, M. Rao, Q. Wang, C. Quan, C. Zhang and Q. Jiang, Synergistic Reinforcement of Polydopamine-Coated Hydroxyapatite and Bmp2 Biomimetic Peptide on the Bioactivity of Pmma-Based Cement, *Compos. Sci. Technol.*, 2016, **123**, 232–240.

9 J. Chen, J. Liu, H. Deng, S. Yao and Y. Wang, Regulatory Synthesis and Characterization of Hydroxyapatite Nanocrystals by a Microwave-Assisted Hydrothermal Method, *Ceram. Int.*, 2020, **46**(2), 2185–2193.

10 X. Hou, K. L. Choy and S. E. Leach, Processing and *in Vitro* Behavior of Hydroxyapatite Coatings Prepared by Electrostatic Spray Assisted Vapor Deposition Method, *J. Biomed. Mater. Res. A*, 2007, **83**(3), 683–691.

11 J. S. Cho, J. C. Lee and S. H. Rhee, Effect of Precursor Concentration and Spray Pyrolysis Temperature Upon Hydroxyapatite Particle Size and Density, *J. Biomed. Mater. Res. B Appl. Biomater.*, 2016, **104**(2), 422–430.

12 G. Liu, X. Geng, H. Pang, X. Li, X. Li, P. Zhu, C. Zhang and H. R. Bakhsheshi Rad, Deposition of Nanostructured Fluorine-Doped Hydroxyapatite Coating from Aqueous Dispersion by Suspension Plasma Spray, *J. Am. Ceram. Soc.*, 2016, **99**(9), 2899–2904.

13 W. H. Lee, C. Y. Loo, A. V. Zavgorodniy and R. Rohanizadeh, High Protein Adsorptive Capacity of Amino Acid-Functionalized Hydroxyapatite, *J. Biomed. Mater. Res. A*, 2013, **101**(3), 873–883.

14 A. Samadikuchaksaraei, M. Gholipourmalekabadi, E. E. Ezadyar, M. Azami, M. Mozafari, B. Johari, S. Kargozar, S. B. Jameie, A. Korourian and A. M. Seifalian, Fabrication And in Vivo evaluation of an Osteoblast-Conditioned Nano-Hydroxyapatite/Gelatin Composite Scaffold for Bone Tissue Regeneration, *J. Biomed. Mater. Res. A*, 2016, **104**(8), 2001–2010.

15 G. O. Mendes, T. Dyer, L. Csetenyi and G. Michael Gadd, Rock Phosphate Solubilization by Abiotic and Fungal-Produced Oxalic Acid: Reaction Parameters and Bioleaching Potential, *Microb. Biotechnol.*, 2021, 1–14.

16 X. Wei and M. Z. Yates, Yttrium-Doped Hydroxyapatite Membranes with High Proton Conductivity, *Chem. Mater.*, 2012, **24**(10), 1738–1743.

17 R. Saha, M. Bose, S. Sen Santara, J. Roy and S. Adak, Identification of Proximal and Distal Axial Ligands in Leishmania Major Pseudoperoxidase, *Biochemistry*, 2013, **52**(49), 8878–8887.

18 P. Suntornsaratoon, N. Charoenphandhu and N. Krishnamra, Fortified Tuna Bone Powder Supplementation Increases Bone Mineral Density of Lactating Rats and Their Offspring, *J. Sci. Food Agric.*, 2018, **98**(5), 2027–2034.

19 O. Coskuner-Weber and V. N. Uversky, Alanine Scanning Effects on the Biochemical and Biophysical Properties of Intrinsically Disordered Proteins: A Case Study of the Histidine to Alanine Mutations in Amyloid-Beta42, *J. Chem. Inf. Model.*, 2019, **59**(2), 871–884.

20 A. Veiga, F. Castro, F. Rocha and A. L. Oliveira, Protein-Based Hydroxyapatite Materials: Tuning Composition toward Biomedical Applications, *ACS Appl. Bio Mater.*, 2020, **3**(6), 3441–3455.

21 K. Mahmud, A. Mitsionis, T. Vaimakis, N. Kourkoumelis and C. Trapalis, The Threonine Effect on Calcium Phosphate Preparation from a Solution Containing Ca/P=1.33 Molar Ratio, *Ceram. Int.*, 2010, **36**(6), 1893–1899.

22 T. Ueatrongchit and Y. Asano, Highly Selective L-Threonine 3-Dehydrogenase from Cupriavidus Necator and Its Use in Determination of L-Threonine, *Anal. Biochem.*, 2011, **410**(1), 44–56.

23 L. Zhu, Y. Fang, Z. Ding, S. Zhang and X. Wang, Developing an L-Threonine-Producing Strain from Wild-Type Escherichia Coli by Modifying the Glucose Uptake, Glyoxylate Shunt, and L-Threonine Biosynthetic Pathway, *Biotechnol. Appl. Biochem.*, 2019, **66**(6), 962–976.

24 Y. Ma, A. Wang, J. Li, Q. li, Q. Han, Y. Chen, S. Wang, X. Zheng, H. Cao and S. Bai, Preparation of Hydroxyapatite with High Surface Area and Dispersity Templated on Calcium Carbonate in Dipeptide Hydrogels, *Colloids Surf., A*, 2020, **596**(124), 740–747.

25 N. I. Ponomareva, T. D. Poprygina, S. I. Karpov, M. V. Lesovoi and B. L. Agapov, Microemulsion Method for Producing Hydroxyapatite, *Russ. J. Gen. Chem.*, 2010, **80**(5), 905–908.

26 S. Y. Park, K. Kim, S. P. Park, Jung H. Lee and H. S. Jung, Aspartic Acid-Assisted Synthesis of Multifunctional Strontium-Substituted Hydroxyapatite Microspheres, *Cryst. Growth Des.*, 2016, **16**(8), 4318–4326.

27 S. Saranya, S. Joseph, S. Justin, R. V. Solomon and P. Wilson, L-Arginine Directed and Ultrasonically Aided Growth of Nanocrystalline Hydroxyapatite Particles with Tunable Morphology, *Colloids Surf., A*, 2018, **538**, 270–279.

28 Y. Guo, J. Lan, C. Zhang, M. Cao, Q. Cai and X. Yang, Mineralization on Polylactide/Gelatin Composite Nanofibers Using Simulated Body Fluid Containing Amino Acid, *Appl. Surf. Sci.*, 2015, **349**, 538–548.

29 S. B. Moussa, H. Bachouâ, M. Gruselle, P. Beaunier, A. Flambard and B. Badraoui, Hybrid Organic-Inorganic Materials Based on Hydroxyapatite Structure, *J. Solid State Chem.*, 2017, **248**, 171–177.

30 T. Matsumoto, M. H. Uddin, S. Hyun An, K. Arakawa, E. Taguchi, A. Nakahira and M. Okazaki, Modulation of Nanotube Formation in Apatite Single Crystal *Via* Organic Molecule Incorporation, *Mater. Chem. Phys.*, 2011, **128**(3), 495–499.

31 G. Zhang, J. Chen, Y. Shen, Q. Yu, Z. Wang and Q. Zhang, Preparation of Amino-Acid-Regulated Hydroxyapatite Particles by Hydrothermal Method, *Mater. Lett.*, 2011, **65**(3), 572–574.